Mean-field models of populations of quadratic integrate-and-fire neurons with noise on the basis of the circular cumulant approach

Cite as: Chaos **31**, 083112 (2021); doi: 10.1063/5.0061575
Submitted: 28 June 2021 · Accepted: 20 July 2021 ·
Published Online: 5 August 2021

Denis S. Goldobin[1,2,a)]

AFFILIATIONS

[1]Institute of Continuous Media Mechanics, UB RAS, Academician Korolev Street 1, 614013 Perm, Russia
[2]Department of Theoretical Physics, Perm State University, Bukirev Street 15, 614990 Perm, Russia

Note: This paper is part of the Focus Issue, In Memory of Vadim S. Anishchenko: Statistical Physics and Nonlinear Dynamics of Complex Systems.
[a)]**Author to whom correspondence should be addressed:** Denis.Goldobin@gmail.com

ABSTRACT

We develop a circular cumulant representation for the recurrent network of quadratic integrate-and-fire neurons subject to noise. The synaptic coupling is global or macroscopically equivalent to it. We assume a Lorentzian distribution of the parameter controlling whether the isolated individual neuron is periodically spiking or excitable. For the infinite chain of circular cumulant equations, a hierarchy of smallness is identified; on the basis of it, we truncate the chain and suggest several two-cumulant neural mass models. These models allow one to go beyond the Ott–Antonsen *Ansatz* and describe the effect of noise on hysteretic transitions between macroscopic regimes of a population with inhibitory coupling. The accuracy of two-cumulant models is analyzed in detail.

Some types of populations of coupled neurons exhibit a surprisingly simple collective behavior. Understanding this simplicity is important both for the macroscopic characterization of neuronal tissues as an active medium and for mathematical modeling of information-processing tasks, which, obviously, cannot be associated with low-dimensional dynamics. The Ott–Antonsen (OA) and Watanabe–Strogatz (WS) theories explained this low dimensionality and gave a mathematical tool for theoretical studies of these populations. In particular, as a rigorous mathematical result, the clusterization dynamics was found to be forbidden by these theories. Later on, a so-called circular cumulant approach was suggested for dealing with imperfect situations, where the conditions of the applicability of the OA theory are violated. The circular cumulant equations allow one to have a theoretical description for low-dimensional macroscopic dynamics, where they remain such beyond the OA theory, or deal with dynamics in higher dimensions, such as the one of clusterization. We present a detailed derivation of the circular cumulant equations for the population of quadratic integrate-and-fire neurons subject to noise and the global synaptic coupling. These equations yield a hierarchy of finite-dimensional neural mass model reductions. We report a set of two-cumulant models and the results on their accuracy for time-independent macroscopic regimes. We also analyze the effect of noise on the multistability between macroscopic states of a population with inhibitory coupling. With the presented technique, one can derive similar equations for other types of coupling, noise, etc.

I. INTRODUCTION

Populations of coupled neuron-like oscillators can demonstrate a surprisingly simple low-dimensional behavior.[1–14] Obviously, no information-processing task can be performed on the basis of such behavior, but it is important for characterization of neural tissues as an active medium. For a vast class of paradigmatic mathematical models, the low dimensionality is dictated by the Ott–Antonsen (OA)[15,16] and Watanabe–Strogatz (WS)[17–19] theories. The understanding of the nature of this low dimensionality can guide the studies aimed at mathematical modeling of complex information-processing behavior, where one can seek to violate the conditions of

the WS/OA theories. For instance, these theories forbid the clusterization dynamics—in the WS systems, the distribution of elements between clusters is frozen in the course of temporal evolution—and reported observations of formation of clusters in Kuramoto-type ensembles were elucidated to emerge as a result of the inaccuracy of numerical integration.[20]

The necessity to generalize the OA theory to the case of populations of neurons, where the conditions of the original OA theory are violated, is an imperative. This generalization is expected to allow one constructing low-dimensional mean-field theories, where they are applicable. Moreover, with this generalization, one might be able to address more intricate issues. While the distribution of elements among clusters is frozen in a perfect case, these clusters will be long-living objects under a weak violation of the OA conditions. This combination of persistence and "plasticity" of clusters can be the basis for some information-processing tasks. Clusterization dynamics, including a particular case as the switching between chimera states, which was a subject of continuous research interest of Vadim S. Anishchenko in recent years,[21–26] were identified to play a role in the functioning of neural tissues (e.g., Refs. 27 and 28). A generalization of the OA theory might provide a mathematical framework for describing this type of dynamics.

One of the primary violations of the OA conditions is the intrinsic noise. The fundamental role of noise for collective dynamics of populations of neurons was identified in Refs. 29 and 30 and studied, e.g., in Refs. 6–10.

A. Quadratic integrate-and-fire neurons with noise

Let us consider the population of quadratic integrate-and-fire neurons (QIFs)[31] with endogenic noise,

$$\dot{V}_j = V_j^2 + I_j, \tag{1}$$

$$I_j = \eta_j + \sigma\zeta_j(t) + Js(t) + I(t), \tag{2}$$

where V_j is the membrane voltage, I_j represents the input current for an individual neuron, η_j is the parameter of an individual neuron (an isolated neuron is excitable for $\eta_j < 0$ and periodically spiking otherwise), $I(t)$ is the external input current, and $\sigma\zeta_j(t)$ are independent Gaussian endogenic (intrinsic) noises: $\langle\zeta_j(t)\,\zeta_m(t+t')\rangle = 2\delta_{jm}\delta(t')$. When V_j reaches $+\infty$, it is reset to $-\infty$, and a synaptic spike is generated.[32] The input synaptic current from other neurons $Js(t)$ is characterized by the coupling coefficient J, which is negative for an inhibitory coupling, and a common field

$$s(t) = \frac{1}{N}\sum_{j=1}^{N}\sum_{n}\delta\left(t - t_j^{(n)}\right),$$

where N is the number of neurons and $t_j^{(n)}$ is the instant of the nth firing event of the jth neuron. In the thermodynamic limit $N \to \infty$, common field $s(t) = r(t)$, where the firing rate $r(t)$ is the probability rate of the finding event of an individual neuron averaged over the population.

One can introduce a phase variable ϕ,

$$V_j = \tan\frac{\phi_j}{2},$$

and rewrite Eq. (1) in its terms,

$$\dot{\phi}_j = (1-\cos\phi_j) + (1+\cos\phi_j)\left[\eta_j + \sigma\zeta_j(t) + Js(t) + I(t)\right]. \tag{3}$$

Let us index the QIFs with the value of their parameter η_j. The Fokker–Planck equation for the probability density $w_\eta(\phi,t)$ of the stochastic system (3) reads

$$\frac{\partial w_\eta}{\partial t} + \frac{\partial}{\partial\phi}\Big(\left[1-\cos\phi + (1+\cos\phi)(\eta + Js + I(t))\right]w_\eta\Big) = \sigma^2\frac{\partial}{\partial\phi}\left((1+\cos\phi)\frac{\partial}{\partial\phi}\left((1+\cos\phi)w_\eta\right)\right). \tag{4}$$

Now, we calculate the firing rate in terms of ϕ. Given the distribution of η is $g(\eta)$, in the thermodynamic limit of a large population, the firing rate equals $r(t) = \int q_\eta(\phi=\pi)\,g(\eta)\,\mathrm{d}\eta$, where q_η is the probability density flux,

$$q_\eta = \left[1-\cos\phi + (1+\cos\phi)(\eta + Js + I(t))\right]w_\eta - \sigma^2(1+\cos\phi)\frac{\partial}{\partial\phi}\left((1+\cos\phi)w_\eta\right).$$

For $\phi = \pi$, the flux $q_\eta(\phi=\pi) = 2w_\eta(\pi)$, and one finds

$$r(t) = \int q_\eta(\pi)\,g(\eta)\mathrm{d}\eta = 2\int w_\eta(\pi)\,g(\eta)\mathrm{d}\eta. \tag{5}$$

The voltage mean field for the η-subpopulation

$$v_\eta = \langle V_\eta\rangle = \text{p.v.}\int_{-\pi}^{\pi}\mathrm{d}\phi\,\tan\frac{\phi}{2}\,w_\eta(\phi). \tag{6}$$

Henceforth, $\langle\cdots\rangle$ indicates an ensemble average.

B. Firing rate and mean voltage dynamics

For Eqs. (1) and (2) with $\sigma = 0$, Montbrió, Pazó, and Roxin (MRP)[5] derived the equations of the mean-field dynamics,

$$\dot{r} = \frac{\Delta}{\pi} + 2rv, \tag{7}$$

$$\dot{v} = v^2 + \eta_0 + Jr + I(t) - \pi^2 r^2, \tag{8}$$

where η_0 and Δ are parameters of the Lorentzian distribution of η_j,

$$g(\eta) = \frac{\pi^{-1}\Delta}{(\eta-\eta_0)^2 + \Delta^2}.$$

The equation system (7) and (8) was shown to be equivalent to the Ott–Antonsen (OA) *Ansatz*.[15,16]

In this paper, our aim is to account for the noise effects,[6–9] and we should go beyond the OA and MPR models. To accomplish this task, one can either employ the "pseudo-cumulant" formalism,[33] constructing a modified neural mass model immediately on the top of the model (7)–(8), or the "circular cumulant" formalism,[34–40] which deals with phase variables ϕ_j and generalizes the OA theory.

Even though the former seems to be more natural for the system (1)–(2), the latter is of vital interest, as the phase-variable and OA approaches are extensively employed for the study of collective dynamics in networks of type-I neurons.[1–4,7–9,41–45]

C. Circular cumulants

The circular cumulants are analogs of conventional cumulants[47,48] of random variables on the infinite real line but for the phase/angular variables on the circumference. We introduce them in association with the Kuramoto–Daido[46] order parameters $z_m = \langle e^{im\phi} \rangle$ as follows. The characteristic function

$$F(k,t) = \langle e^{ke^{i\phi}} \rangle = \sum_{m=0}^{\infty} z_m(t) \frac{k^m}{m!}$$

serves as the generating function for moments z_m. We define the cumulant-generating function as

$$\Psi(k,t) = k\frac{\partial}{\partial k} \ln F(k,t) = \sum_{m=1}^{\infty} \kappa_m(t) k^m,$$

where κ_m are circular cumulants. For instance, the first three cumulants are

$$\kappa_1 = z_1, \quad \kappa_2 = z_2 - z_1^2, \; \kappa_3 = \frac{z_3 - 3z_2z_1 + 2z_1^3}{2}.$$

Here, the first element is just the Kuramoto order parameter, and the second element measures the deviation of z_2 from z_1^2, which would correspond to the OA *Ansatz*, $z_m = z_1^m$. For the OA *Ansatz*, $\kappa_1 = z_1$ and $\kappa_{m>1} = 0$, which makes the circular cumulants a natural framework for dealing with the dynamics deviating from the OA theory.

In this paper, we present a generation of low-dimensional neural mass models based on two-cumulant reductions (Sec. II A), report the effect of noise on the bistability between time-independent states of the QIF network with global synaptic coupling (1) and (2) (Sec. II B), and analyze the accuracy of these model reductions (Sec. II C). In Sec. III, we provide a regular derivation of the infinite chain of equations for circular cumulants κ_m and substantiate the truncations of this chain. The calculation of the firing rate with circular cumulants is discussed in Sec. III G. Conclusions are drawn in Sec. IV.

II. RESULTS

A. Two-cumulant reductions

In this section, we present low-dimensional model reductions for the macroscopic dynamics of noisy QIF populations; the derivation is provided in Sec. III. The mean-field models beyond the Ott–Antonsen *Ansatz* can be formulated in terms of order parameters for phases ϕ_j. For the firing rate and the ensemble-mean voltage, one can find (see Refs. 8, 9, and 36 or Sec. III G)

$$\pi r(t) - iv(t) = \frac{1-Z}{1+Z} + \frac{2\kappa_2}{(1+Z)^3} + \mathcal{O}(\kappa_2^2, \kappa_3), \tag{9}$$

where Kuramoto order parameter $Z = z_1 = \kappa_1$. For an enhanced accuracy (e.g., the "Gaussian-friendly" closure[35]),

$$\pi r(t) - iv(t) = \frac{1-Z}{1+Z} + \frac{2\kappa_2}{(1+Z)^3} - \frac{6\kappa_2^2}{Z(1+Z)^5} + \mathcal{O}(\sigma^6). \tag{10}$$

Two generic two-cumulant reductions can be suggested for the Lorentzian distribution $g(\eta) = \Delta/[\pi\{(\eta-\eta_0)^2 + \Delta^2\}]$, where η_0 is the distribution median and Δ is the half width at half maximum.

(i) The minimalistic two-cumulant reduction:

$$\dot{Z} = (i\Omega_{\eta_0} - \Delta)Z + h\left(1 + \kappa_2 + Z^2\right) - \frac{\sigma^2}{2}(1+Z)^3, \tag{11}$$

$$\dot{\kappa}_2 = 2(i\Omega_{\eta_0} - \Delta)\kappa_2 + 4hZ\kappa_2 - \frac{\sigma^2}{2}(1+Z)^4 - 6\sigma^2(1+Z)^2\kappa_2, \tag{12}$$

where

$$\Omega_{\eta_0} = \eta_0 + Js + I(t) + 1, \quad h = \frac{i\left(\eta_0 + Js + I(t) - 1\right) - \Delta}{2}.$$

This reduction is obtained from two first circular cumulant equations (22) and (23) by neglecting all higher cumulants $\kappa_{n\geq 2}$ and as much smaller terms [like the $\sigma^2\kappa_2^2$-term in (23)] as possible. The "strong" inaccuracy of this truncation is $\mathcal{O}(\sigma^4)$. Nonetheless, we keep the $\sigma^2 Z^n \kappa_2$-terms in (12) as they maintain the "dissipativeness" of the dynamics of κ_2 for homogeneous populations ($\Delta = 0$), even though these terms are small, $\sim\sigma^4$. This model is equivalent to the model of Ref. 8 in the limit of zero spike duration.

(ii) Two-cumulant reduction compatible with the wrapped Gaussian distribution of phases,[35] i.e., based on the closures $\kappa_3 = (3/2)\kappa_2^2/\kappa_1$ and $\kappa_4 = (8/3)\kappa_2^3/\kappa_1^2$, which follow from the algebraic relations between the circular cumulants of a wrapped Gaussian distribution,

$$\dot{Z} = (i\Omega_{\eta_0} - \Delta)Z + h\left(1 + \kappa_2 + Z^2\right) - \sigma^2\left(\frac{1}{2}(1+Z)^3 + \frac{3}{2}(1+Z)\kappa_2 + \frac{3}{2}\frac{\kappa_2^2}{Z}\right), \tag{13}$$

$$\dot{\kappa}_2 = 2(i\Omega_{\eta_0} - \Delta)\kappa_2 + h\left(6\frac{\kappa_2^2}{Z} + 4Z\kappa_2\right) - \sigma^2\left(\frac{1}{2}(1+Z)^4 + 6(1+Z)^2\kappa_2 + 15\frac{\kappa_2^2}{Z} + \frac{39}{2}\kappa_2^2 + 24\frac{\kappa_2^3}{Z^2}\right). \tag{14}$$

In Sec. III, we additionally provide more sophisticated model reductions, which can be less practical because of their complexity.

B. Macroscopic dynamics of globally coupled QIFs

In Fig. 1, one can see the hysteretic transitions between two coexisting regimes with high and low firing rates, previously reported[5] for the noise-free case. The bistability domain is diminished by the noise. The impact of noise on the high firing rate regime and the left boundary of the bistability domain is weak. The

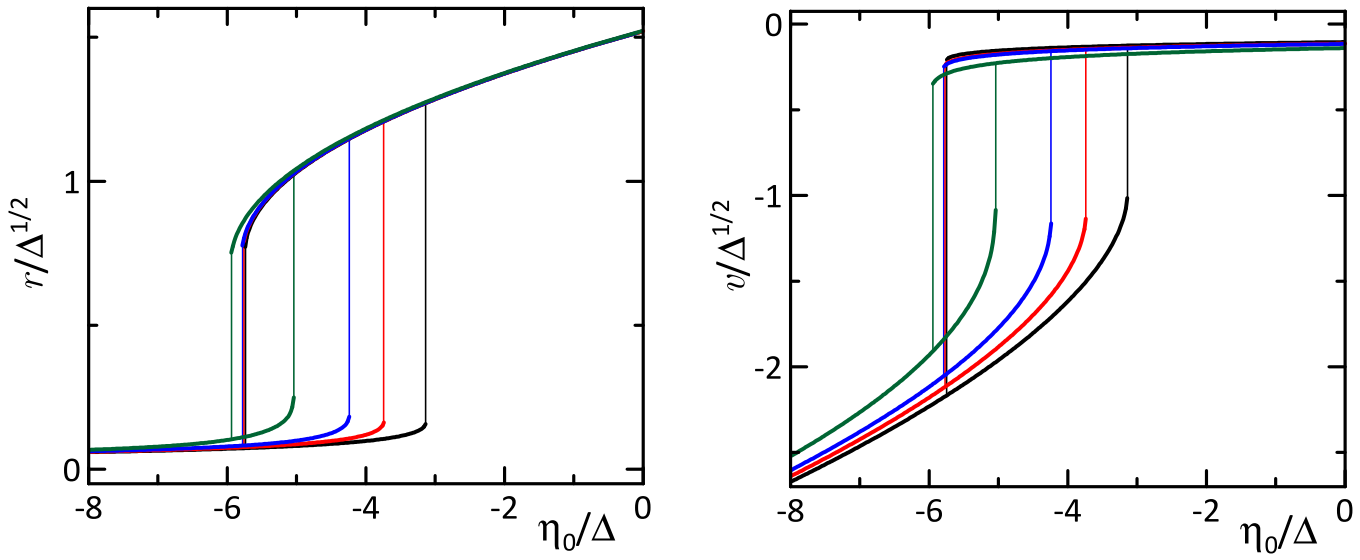

FIG. 1. Stable states are plotted with black lines for the noise-free case and $J/\Delta^{1/2} = 15$. The bistability domain monotonously shrinks as the noise intensity increases: $\sigma^2/\Delta^{3/2} = 0.8$ (red), 1.6 (blue), and 3.2 (green). This is an "exact" numeric solution with system (17).

low firing rate regime is influenced much stronger; noise expectedly induces additional firing events and increases the firing rate. The domain of the low firing rate regime is significantly diminished, and the right boundary of the bistability domain is shifted. In Fig. 2, the effect of noise on the bistability domain is presented in the entire parameter space.

One can see that the two-cumulant model reductions are reasonably accurate even for as strong noise as $\sigma/\Delta^{3/4} = 1$. Notice that the results are typically especially sensitive to inaccuracies close to the bifurcation curves, and the bistability domain is bounded by the saddle-node bifurcation curves.

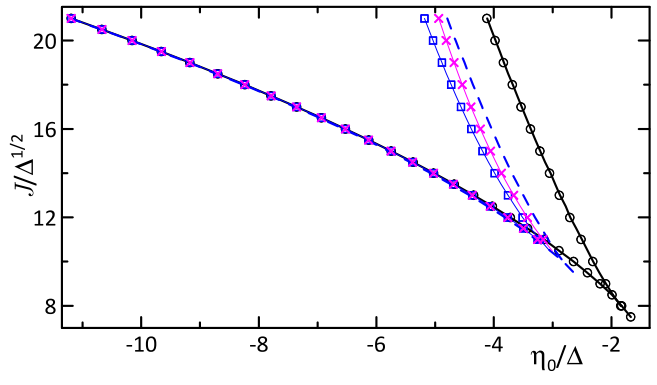

FIG. 2. The bistability between two regimes occurs within the cusp. Black solid lines: the "exact" solution for $\sigma/\Delta^{3/4} = 0.1$; blue dashed lines: the "exact" solution for $\sigma/\Delta^{3/4} = 1$; circles and squares: the results for the C2e model reduction; and crests: C3s model reduction for $\sigma/\Delta^{3/4} = 1$. The C3s model results are not shown for $\sigma/\Delta^{3/4} = 0.1$ as the discrepancy between the model reduction and the "exact" solution cannot be seen even for circles.

C. Accuracy of model reductions

Here, we report the accuracy analysis for the macroscopic model reductions:

(OA) the Ott–Antonsen *Ansatz*, where in Eqs. (11) and (9), one sets $\kappa_2 = 0$ [this corresponds to *Ansatz* $z_m = Z^m$ in Eq. (17) for $m = 1$];

(C20) the minimalistic two-cumulant approximation (11) and (12) with (9);

(C2e) the enhanced two-cumulant approximation (26) and (27) with (9);

(C2G) the two-cumulant approximation (13) and (14) with (10), which can accurately embed the wrapped Gaussian distribution; and

(C3s) the two-cumulant approximation (32) and (33) with quasi-static approximation (30) for κ_3 and firing rate (31).

The accuracy and applicability of five reductions are examined for macroscopic regimes presented in Fig. 1. First, we demonstrate the relevance of the cumulant expansion for both weak and moderate noise; in Fig. 3(a), one can see well pronounced hierarchies of cumulants for $\sigma/\Delta^{3/4} = 0.1$ and 1. Second, the accuracy of Z for the solutions is plotted in Fig. 3(b). The "exact" solution is calculated with system (17) and 200 elements z_m for the rhs- and 1200 elements for the lhs-branch solution (usage of less than half of this number of elements is insufficient for a uniformly accurate calculation of the results plotted in the parameter domain of Figs. 1 and 2).

The results of the accuracy analysis are summarized in Fig. 4. The simplest two-cumulant reduction (C20) fails for some regimes in the presence of strong noise; the enhanced minimalistic two-cumulant reduction (C2e) and the Gaussian-friendly approximation

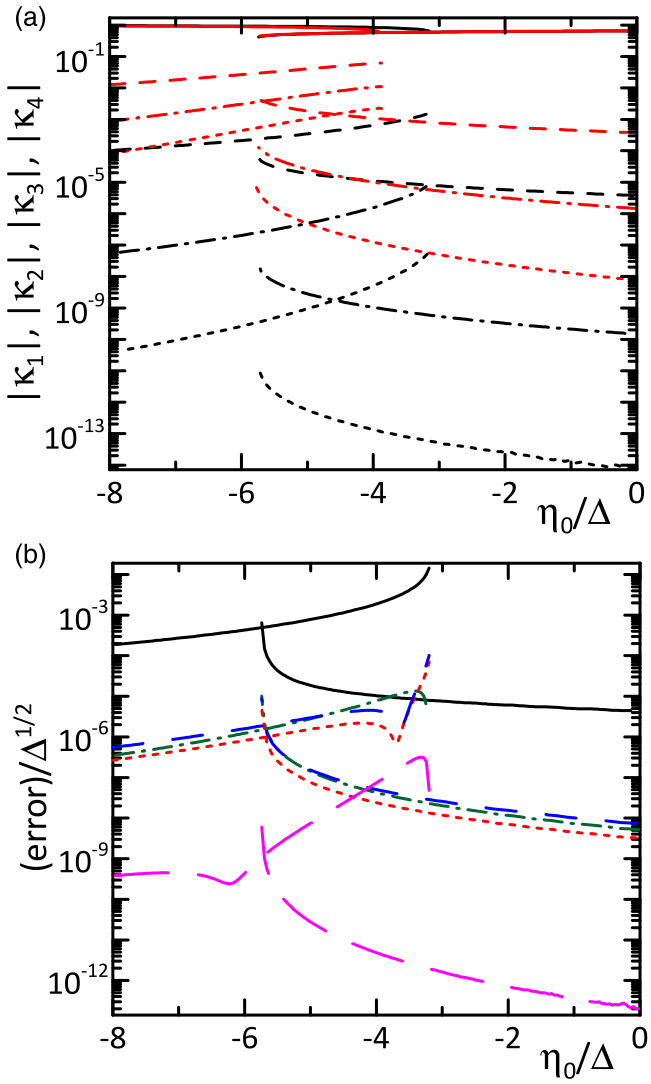

FIG. 3. (a) First four cumulants $\kappa_1 = Z$ (solid lines), κ_2 (dashed lines), κ_3 (dashed–dotted lines), and κ_4 (dotted lines) exhibit a well pronounced hierarchy of smallness for $\sigma/\Delta^{3/4} = 0.1$ (black) and 1 (red); parameter $J/\Delta^{1/2} = 15$. Two sets of curves are plotted for the left and right branches of the solution. (b) The accuracy of reduced models is presented for $\sigma/\Delta^{3/4} = 0.1$; black solid lines: OA, blue dashed: C20, red dotted: C2e, green dashed–dotted: C2G, and magenta long-dashed: C3s.

(C2G) are optimal since they remain reasonably accurate even for strong noise. Notice that the OA *Ansatz* turns out to be inaccurate already for $\sigma/\Delta^{3/4} > 0.1$.

III. METHODS

In this section, we project the Fokker–Planck equation (4) onto the Fourier basis, show that one can adopt a Lorentzian distribution $g(\eta)$ and use the residue theorem (which is more

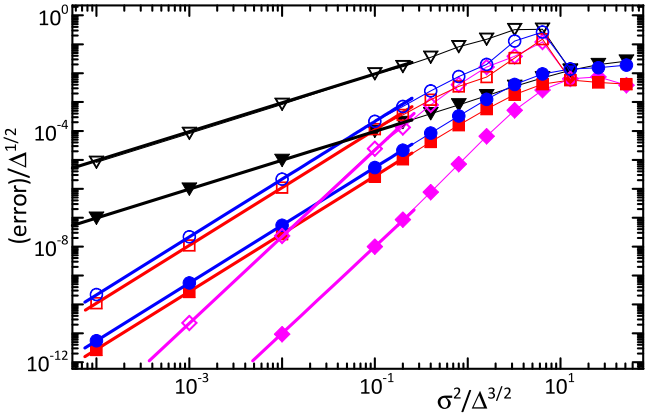

FIG. 4. The inaccuracy of model reductions is plotted vs σ^2 for the lhs- (open symbols) and rhs-branch solutions (filled symbols) at $J/\Delta^{1/2} = 15$; black triangles: OA, blue circles: C20, red squares: C2e, and magenta diamonds: C3s. For the rhs-branch solution, the error is averaged over $\eta_0/\Delta \in [-5.5, 0]$ [see the dependence of error on η_0 in Fig. 3(b)]. For the lhs-one, the averaging interval is for $\eta_0/\Delta > -8$. Above $\sigma^2/\Delta^{3/2} \approx 10$, the bistability between two macroscopic regimes disappears. The bold solid lines indicate the small-σ power laws: $\propto \sigma^2$ for OA, $\propto \sigma^4$ for C20, and C2e, $\propto \sigma^6$ for C3s.

sophisticated in this case than usually for the Ott–Antonsen equations), and recast the equations in terms of circular cumulants. Some laborious technical calculations are provided here as well.

A. Fokker–Planck equation

Equation (4) can be recast as

$$\frac{\partial w_\eta}{\partial t} + \frac{\partial}{\partial \phi}\left(\left[\Omega_\eta - i h_\eta e^{-i\phi} + i h_\eta^* e^{i\phi}\right] w_\eta\right) = \sigma^2 \frac{\partial}{\partial \phi}\left(\left[\sin\phi + \frac{1}{2}\sin 2\phi\right] w_\eta + \frac{\partial}{\partial \phi}\left[\left(\frac{3}{2} + 2\cos\phi + \frac{1}{2}\cos 2\phi\right) w_\eta\right]\right), \tag{15}$$

where

$$\Omega_\eta \equiv \eta + Js + I(t) + 1, \quad h_\eta \equiv \frac{i}{2}(\eta + Js + I(t) - 1).$$

In the Fourier space, $w_\eta(\phi, t) = \frac{1}{2\pi}\left[1 + \sum_{m=1}^{\infty}(a_m(t)e^{-im\phi} + c.c.)\right]$, where "*c.c.*" stands for complex conjugate, and Eq. (15) takes the form

$$\dot{a}_m(\eta) = m\left(i\Omega_\eta a_m + h_\eta a_{m-1} - h_\eta^* a_{m+1} + \frac{\sigma^2}{2}a_{m-1} - \frac{\sigma^2}{2}a_{m+1} + \frac{\sigma^2}{4}a_{m-2} - \frac{\sigma^2}{4}a_{m+2}\right) - m^2\sigma^2\left(\frac{3}{2}a_m + a_{m-1} + a_{m+1} + \frac{1}{4}a_{m-2} + \frac{1}{4}a_{m+2}\right)$$

or

$$\dot{a}_m(\eta) = m\left(i\Omega_\eta a_m + h_\eta a_{m-1} - h_\eta^* a_{m+1}\right) - \sigma^2\left(\frac{3}{2}m^2 a_m + \left(m^2 - \frac{m}{2}\right)a_{m-1} + \left(m^2 + \frac{m}{2}\right)a_{m+1} + \frac{m(m-1)}{4}a_{m-2} + \frac{m(m+1)}{4}a_{m+2}\right). \tag{16}$$

Here, by definition, $a_0 = 1$ and $a_{-m} = a_m^*$.

The net probability density $w(\phi, t) = \int w_\eta(\phi, t)\, g(\eta)\mathrm{d}\eta$, and the ensemble Kuramoto–Daido[46] order parameters

$$z_m = \int a_m(\eta)\, g(\eta)\mathrm{d}\eta.$$

B. Lorentzian distribution of η

Let us assume smoothness of $a_m(\eta, t = 0)$ as functions of η and construct the analytical continuation of $a_m(\eta)$ into the complex plane η. Given the initial conditions $\{a_m(\eta, 0),\ m = 1, 2, \dots\}$ are analytical functions of η, the set $\{a_m(\eta, t),\ m = 1, 2, \dots\}$ governed by the equation system (16) preserves analyticity. Notice that for $m = 1$, the term $a_{m-2} = a_{-1} = a_1^*$ would break the analyticity of system (16) if the coefficient ahead of this term, $m(m-1)/4$, were not zero for $m = 1$.

Furthermore, specifically with $\Omega_\eta = \eta + Js + I(t) + 1$ and $h_\eta = \frac{i}{2}(\eta + Js + I(t) - 1)$, for $\eta = \eta_r + i\eta_i$, Eq. (16) yields

$$\dot{a}_m(\eta_r + i\eta_i) = -m\,(\eta_i - i\eta_r)\left(a_m + \frac{a_{m-1} + a_{m+1}}{2}\right) + m\left(i\Omega_0 a_m + h_0 a_{m-1} - h_0^* a_{m+1}\right) - \sigma^2\mathcal{O}(a_m);$$

i.e., $a_m(\eta)$ tends to $(-1)^m$ on the upper arc. [More strictly, for $|\eta| \to \infty$, one can neglect the terms without η, which yield the Ott–Antonsen form of equations. On the Ott–Antonsen manifold, $a_m = a_1^m$, and one finds $\dot{a}_1 = \frac{i\eta}{2}(1 + a_1)^2$, which yields the fixed point $a_1 = -1$, and this fixed point is (nonlinearly) attracting within the physical domain $|a_1| \le 1$ for $\mathrm{Im}\,\eta \ge 0$; for $\mathrm{Im}\,\eta < 0$, the trajectories leave the physical domain and run to infinity.] Hence, for $g(\eta) = \frac{\Delta}{\pi[(\eta-\eta_0)^2+\Delta^2]}$, one can calculate z_m via residues,[49–51]

$$z_m = \int a_m(\eta)\, g(\eta)\mathrm{d}\eta = a_m(\eta_0 + i\Delta).$$

Thus, one finds from Eq. (16) for the ensemble order parameters,

$$\dot{z}_m = m\left((i\Omega_{\eta_0} - \Delta)z_m + h_{\eta_0} z_{m-1} - h_{\eta_0}^* z_{m+1} - \frac{\Delta + \sigma^2}{2}(z_{m-1} + z_{m+1})\right) - \sigma^2\left(\frac{3m^2}{2}z_m + m(m-1)z_{m-1} + m^2 z_{m+1} + \frac{m(m-1)}{4}z_{m-2} + \frac{m(m+1)}{4}z_{m+2}\right).$$

With

$$h_{\eta_0} - \frac{\Delta + \sigma^2}{2} \equiv \mathcal{H} = \frac{i(\eta_0 + Js + I(t) - 1) - (\Delta + \sigma^2)}{2},$$

these equations read

$$\dot{z}_m = m\left((i\Omega_{\eta_0} - \Delta)z_m + \mathcal{H}(z_{m-1} + z_{m+1})\right) - \sigma^2\left(\frac{3}{2}m^2 z_m + m(m-1)z_{m-1} + m^2 z_{m+1} + \frac{m(m-1)}{4}z_{m-2} + \frac{m(m+1)}{4}z_{m+2}\right). \tag{17}$$

C. Generating function dynamics

For the generating function $F(k, t) = \sum_{m=0}^{\infty} z_m(t)\frac{k^m}{m!}$, equation system (17) yields $\frac{\partial}{\partial t}F(k, t)$. For term mz_m, one can find $k\frac{\partial}{\partial k}F = \sum_{m=0}^{\infty} mz_m\frac{k^m}{m!}$; for mz_{m-1}, kF; for mz_{m+1}, $k\frac{\partial^2}{\partial k^2}F = \sum_{m=0}^{\infty} km(m-1)z_m\frac{k^{m-2}}{m!} = \sum_{m=0}^{\infty} mz_{m+1}\frac{k^m}{m!}$; for $m^2 z_m$, $k\frac{\partial}{\partial k}\left(k\frac{\partial}{\partial k}F\right)$; for $m(m-1)z_{m-1}$, $k^2\frac{\partial}{\partial k}F = \sum_{m=0}^{\infty} k^2 mz_m\frac{k^{m-1}}{m!} = \sum_{m=0}^{\infty} m(m-1)z_{m-1}\frac{k^m}{m!}$; for $m^2 z_{m+1}$, $k\frac{\partial}{\partial k}\left(k\frac{\partial^2}{\partial k^2}F\right) = \sum_{m=0}^{\infty} m(m-1)^2 z_m\frac{k^{m-1}}{m!} = \sum_{m=0}^{\infty} m^2 z_{m+1}\frac{k^m}{m!}$; for $m(m-1)z_{m-2}$, k^2F; for $m(m+1)z_{m+2}$, $k\frac{\partial^2}{\partial k^2}\left(k\frac{\partial^2}{\partial k^2}F\right) = \sum_{m=0}^{\infty} m(m-1)^2(m-2)z_m\frac{k^{m-2}}{m!} = \sum_{m=0}^{\infty} m(m+1)z_{m+2}\frac{k^m}{m!}$.

Thus,

$$\frac{\partial F}{\partial t} = (i\Omega_{\eta_0} - \Delta)k\frac{\partial F}{\partial k} + \mathcal{H}\left(kF + k\frac{\partial^2 F}{\partial k^2}\right) - \sigma^2\left(\frac{3}{2}k\frac{\partial}{\partial k}\left(k\frac{\partial F}{\partial k}\right) + k^2\frac{\partial F}{\partial k} + k\frac{\partial}{\partial k}\left(k\frac{\partial^2 F}{\partial k^2}\right) + \frac{1}{4}\left[k^2 F + k\frac{\partial^2}{\partial k^2}\left(k\frac{\partial^2 F}{\partial k^2}\right)\right]\right).$$

For "circular cumulants," we introduce $\Psi = k\frac{\partial}{\partial k}\ln F = \frac{k}{F}\frac{\partial F}{\partial k} = \sum_{m=1}^{\infty}\kappa_m(t)\,k^m$, $\frac{\partial}{\partial t}\Psi = k\frac{\partial}{\partial k}\left(\frac{1}{F}\frac{\partial F}{\partial t}\right)$, and

$$\frac{\partial\Psi}{\partial t} = k\frac{\partial}{\partial k}\left[(i\Omega_{\eta_0} - \Delta)\Psi + \mathcal{H}\left(k + \frac{\left(k\frac{\partial}{\partial k} - 1\right)\Psi + \Psi^2}{k}\right) - \sigma^2\left\{\frac{3}{2}\left(k\frac{\partial\Psi}{\partial k} + \Psi^2\right) + k\Psi + \frac{\left(k\frac{\partial}{\partial k} - 1\right)^2\Psi + \left(\frac{3}{2}k\frac{\partial}{\partial k} - 2\right)\Psi^2 + \Psi^3}{k} + \frac{k^2}{4} + \frac{\left(k\frac{\partial}{\partial k} - 1\right)^2\left(k\frac{\partial}{\partial k} - 2\right)\Psi + \left[2\left(k\frac{\partial}{\partial k}\right)^2 - 6k\frac{\partial}{\partial k} + 5\right]\Psi^2 - \left(k\frac{\partial}{\partial k}\Psi\right)^2 + \left(2k\frac{\partial}{\partial k} - 4\right)\Psi^3 + \Psi^4}{4k^2}\right\}\right]. \tag{18}$$

With expansion $\Psi = \sum_{m=1}^{\infty} \kappa_m k^m$, Eq. (18) yields

$$\dot{\kappa}_m = m\Bigg[(i\Omega_{\eta_0} - \Delta)\kappa_m + \mathcal{H}\left(\delta_{1m} + m\kappa_{m+1} + \sum_{\substack{m_1+m_2\\=m+1}} \kappa_{m_1}\kappa_{m_2}\right) - \sigma^2\left(\frac{3}{2}m\kappa_m + \frac{3}{2}\sum_{\substack{m_1+m_2\\=m}} \kappa_{m_1}\kappa_{m_2} + (1-\delta_{1m})\kappa_{m-1}\right.$$
$$+ m^2\kappa_{m+1} + \frac{3m-1}{2}\sum_{\substack{m_1+m_2\\=m+1}} \kappa_{m_1}\kappa_{m_2} + \sum_{\substack{m_1+m_2+m_3\\=m+1}} \kappa_{m_1}\kappa_{m_2}\kappa_{m_3} + \frac{1}{4}\delta_{2m} + \frac{m(m+1)^2}{4}\kappa_{m+2}$$
$$\left.+ \sum_{\substack{m_1+m_2\\=m+2}} \frac{2m^2+2m+1-m_1m_2}{4}\kappa_{m_1}\kappa_{m_2} + \frac{m}{2}\sum_{\substack{m_1+m_2+m_3\\=m+2}} \kappa_{m_1}\kappa_{m_2}\kappa_{m_3} + \frac{1}{4}\sum_{\substack{m_1+m_2+m_3\\+m_4=m+2}} \kappa_{m_1}\kappa_{m_2}\kappa_{m_3}\kappa_{m_4}\right)\Bigg]. \tag{19}$$

Alternatively, with $h \equiv h_{\eta_0} - \frac{\Delta}{2} = \frac{i(\eta_0+Js+I(t)-1)-\Delta}{2}$,

$$\dot{\kappa}_m = m\Bigg[(i\Omega_{\eta_0} - \Delta)\kappa_m + h\left(\delta_{1m} + m\kappa_{m+1} + \sum_{\substack{m_1+m_2\\=m+1}} \kappa_{m_1}\kappa_{m_2}\right) - \sigma^2\left(\frac{3}{2}m\kappa_m + \frac{3}{2}\sum_{\substack{m_1+m_2\\=m}} \kappa_{m_1}\kappa_{m_2}\right.$$
$$+ (1-\delta_{1m})\kappa_{m-1} + \frac{\delta_{1m}}{2} + \left(m^2 + \frac{m}{2}\right)\kappa_{m+1} + \frac{3m}{2}\sum_{\substack{m_1+m_2\\=m+1}} \kappa_{m_1}\kappa_{m_2} + \sum_{\substack{m_1+m_2+m_3\\=m+1}} \kappa_{m_1}\kappa_{m_2}\kappa_{m_3} + \frac{1}{4}\delta_{2m} + \frac{m(m+1)^2}{4}\kappa_{m+2}$$
$$\left.+ \sum_{\substack{m_1+m_2\\=m+2}} \frac{2m^2+2m+1-m_1m_2}{4}\kappa_{m_1}\kappa_{m_2} + \frac{m}{2}\sum_{\substack{m_1+m_2+m_3\\=m+2}} \kappa_{m_1}\kappa_{m_2}\kappa_{m_3} + \frac{1}{4}\sum_{\substack{m_1+m_2+m_3\\+m_4=m+2}} \kappa_{m_1}\kappa_{m_2}\kappa_{m_3}\kappa_{m_4}\right)\Bigg]. \tag{20}$$

For some considerations, it might be more convenient to rearrange the sums in the latter equation. In terms of $\kappa'_m \equiv \delta_{1m} + \kappa_m$, i.e., only the first cumulant is shifted, $1 + \kappa_1 = \kappa'_1$, one finds a more concise form of equations,

$$\dot{\kappa}'_m = m\Bigg[(i\Omega_{\eta_0} - \Delta)(\kappa'_m - \delta_{1m}) + h\left(m\kappa'_{m+1} + 2\delta_{1m} - 2\kappa'_m + \sum_{\substack{m_1+m_2\\=m+1}} \kappa'_{m_1}\kappa'_{m_2}\right) - \sigma^2\left(\frac{m(m+1)^2}{4}\kappa'_{m+2}\right.$$
$$\left.+ \sum_{\substack{m_1+m_2\\=m+2}} \frac{2m^2+2m+1-m_1m_2}{4}\kappa'_{m_1}\kappa'_{m_2} + \frac{m}{2}\sum_{\substack{m_1+m_2+m_3\\=m+2}} \kappa'_{m_1}\kappa'_{m_2}\kappa'_{m_3} + \frac{1}{4}\sum_{\substack{m_1+m_2+m_3\\+m_4=m+2}} \kappa'_{m_1}\kappa'_{m_2}\kappa'_{m_3}\kappa'_{m_4}\right)\Bigg]. \tag{21}$$

Here, the noise-terms are noticeably homogeneous: the sum of their indices in all sums $\sum \kappa'_{m_1}\cdots\kappa'_{m_n}$ is the same, $m_1 + \cdots + m_n = m + 2$. This is important for a systematic analysis of geometric smallness hierarchies $\kappa'_m \sim \varepsilon^{m-1}\kappa'_1$ with various values of small parameter ε, which often appear for circular cumulant series.[36]

For the dynamics of the first four cumulants,

$$\dot{\kappa}_1 = (i\Omega_{\eta_0} - \Delta)\kappa_1 + h\left(1 + \kappa_2 + \kappa_1^2\right) - \sigma^2\left(\frac{(1+\kappa_1)^3}{2} + \frac{3}{2}(1+\kappa_1)\kappa_2 + \kappa_3\right), \tag{22}$$

$$\dot{\kappa}_2 = 2(i\Omega_{\eta_0} - \Delta)\kappa_2 + 4h\left(\kappa_3 + \kappa_1\kappa_2\right) - 2\sigma^2\left(\frac{(1+\kappa_1)^4}{4} + 3(1+\kappa_1)^2\kappa_2 + 5(1+\kappa_1)\kappa_3 + \frac{9}{4}\kappa_2^2 + \frac{9}{2}\kappa_4\right), \tag{23}$$

$$\dot{\kappa}_3 = 3(i\Omega_{\eta_0} - \Delta)\kappa_3 + 3h\left(3\kappa_4 + 2\kappa_1\kappa_3 + \kappa_2^2\right) - 3\sigma^2\left((1+\kappa_1)^3\kappa_2 + \frac{9}{2}(1+\kappa_1)^2\kappa_3 + \frac{9}{2}(1+\kappa_1)\kappa_2^2 + \frac{21}{2}(1+\kappa_1)\kappa_4 + \frac{19}{2}\kappa_2\kappa_3 + 12\kappa_5\right), \tag{24}$$

$$\dot{\kappa}_4 = 4(i\Omega_{\eta_0} - \Delta)\kappa_4 + 8h\,(2\kappa_5 + \kappa_1\kappa_4 + \kappa_2\kappa_3) - 4\sigma^2\left((1+\kappa_1)^4\kappa_3 + \frac{3}{2}(1+\kappa_1)^2\kappa_2^2 + 6(1+\kappa_1)^2\kappa_4 + 18(1+\kappa_1)\kappa_5 + 12(1+\kappa_1)\kappa_2\kappa_3 + 2\kappa_2^3 + 8\kappa_3^2 + \frac{33}{2}\kappa_2\kappa_4 + 25\kappa_6\right). \quad (25)$$

Let us assess the orders of smallness of high-order cumulants for $\kappa_1 \sim 1$ and $\sigma^2 \ll 1$, with the assumption that the reference value of κ_{m+1} is nonlarger than that of κ_m. Equation (23) dictates for small κ_2 the order of magnitude $\kappa_2 \sim \sigma^2$. Furthermore, $\kappa_3 \sim \max\{\kappa_2^2, \sigma^2\kappa_2\}$; i.e., $\kappa_3 \sim \sigma^4$. Generally, one can substitute the hierarchy $\kappa_m \sim \sigma^{2(m-1)}$ to Eq. (19) and see that it is admissible.

Alternatively, if, due to some reason, $\kappa_1 \sim \varepsilon \ll 1$, then, according to (23), $\kappa_2 \sim \sigma^2$; according to (24), $\kappa_3 \sim \sigma^4$; generally, $\kappa_{m\geq 2} \sim \sigma^{2(m-1)}$. Thus, we have the same hierarchy, as for $\kappa_1 \sim 1$. This smallness hierarchy allows us to construct finite-cumulant model reductions by truncating the infinite chain of cumulant equations.

D. Plain two-cumulant reduction with $\kappa_3 = \kappa_4 = 0$

A plain first order correction to the OA *Ansatz* for $Z = \kappa_1$ and κ_2 yields

$$\dot{Z} = (i\Omega_{\eta_0} - \Delta)Z + h\left(1 + \kappa_2 + Z^2\right) - \sigma^2\left(\frac{1}{2}(1+Z)^3 + \frac{3}{2}(1+Z)\kappa_2\right), \quad (26)$$

$$\dot{\kappa}_2 = 2(i\Omega_{\eta_0} - \Delta)\kappa_2 + 4hZ\kappa_2 - 2\sigma^2\left(\frac{1}{4}(1+Z)^4 + 3(1+Z)^2\kappa_2 + \frac{9}{4}\kappa_2^2\right). \quad (27)$$

The "strong" inaccuracy of this truncation is $\mathcal{O}(\sigma^4)$ for the dynamics of κ_2 [see Eq. (23) and note $\kappa_3 \sim \sigma^4$, $\kappa_4 \sim \sigma^6$]; thus [see Eq. (22)], the same inaccuracy $\mathcal{O}(\sigma^4)$ is introduced into the dynamics of κ_1. Here, the terms with the factor $\sigma^2\kappa_2$ can be omitted due to the hierarchy $\kappa_m \sim \sigma^{2(m-1)}$. However, we keep these terms, as they create the dissipativity of the dynamics of κ_2, which can be lost for homogeneous populations ($\Delta = 0$) otherwise. For $\sigma^2 \ll \Delta$, the $\sigma^2\kappa_2$-terms can be omitted as well.

E. Two-cumulant reduction consistent with a wrapped Gaussian distribution

With $\kappa_3 = (3/2)\kappa_2^2/Z$ and $\kappa_4 = (8/3)\kappa_2^3/Z^2$ suggested by the wrapped Gaussian distribution,[35]

$$\dot{Z} = (i\Omega_{\eta_0} - \Delta)Z + h\left(1 + \kappa_2 + Z^2\right) - \sigma^2\left(\frac{1}{2}(1+Z)^3 + \frac{3}{2}(1+Z)\kappa_2 + \frac{3}{2}\frac{\kappa_2^2}{Z}\right), \quad (28)$$

$$\dot{\kappa}_2 = 2(i\Omega_{\eta_0} - \Delta)\kappa_2 + h\left(6\frac{\kappa_2^2}{Z} + 4Z\kappa_2\right) - 2\sigma^2\left(\frac{1}{4}(1+Z)^4 + 3(1+Z)^2\kappa_2 + \frac{15}{2}\frac{\kappa_2^2}{Z} + \frac{39}{4}\kappa_2^2 + 12\frac{\kappa_2^3}{Z^2}\right). \quad (29)$$

F. Two-cumulant reduction with quasi-static approximation for third cumulant κ_3

In Eqs. (22)–(25), one can see that the relaxation dynamics of κ_n becomes faster for higher n. Even for regimes of macroscopic oscillations, the dynamics of higher-order cumulants can be the dynamics of fast relaxation to the values enslaved by the few leading cumulants. Hence, one can consider the model reduction where κ_3 is approximately determined from Eq. (24) with quasi-static assumption and only the leading terms are kept,

$$0 \approx 3(i\Omega_{\eta_0} - \Delta)\kappa_3 + 3h(r_2)\left(2\kappa_1\kappa_3 + \kappa_2^2\right) - 3\sigma^2\left((1+\kappa_1)^3\kappa_2 + \frac{9}{2}(1+\kappa_1)^2\kappa_3 + \frac{9}{2}(1+\kappa_1)\kappa_2^2\right),$$

i.e.,

$$\kappa_3 \approx \frac{h(r_2)\kappa_2^2 - \sigma^2\left((1+Z)^3\kappa_2 + \frac{9}{2}(1+Z)\kappa_2^2\right)}{-i\Omega_{\eta_0} + \Delta - 2h(r_2)Z + \frac{9}{2}\sigma^2(1+Z)^2}, \quad (30)$$

where in $h(r_2)$, the firing rate is calculated with Z, κ_2 only [Eq. (9)]. Furthermore, one employs κ_3 for calculation of firing rate r_3,

$$\pi r_3(t) - iv_3(t) = \frac{1-Z}{1+Z} + \frac{2\kappa_2}{(1+Z)^3} + \frac{6\kappa_2^2}{(1+Z)^5} - \frac{4\kappa_3}{(1+Z)^4}, \quad (31)$$

and substitute it into Eqs. (22) and (23) with $\kappa_{n>3}$ set to 0,

$$\dot{Z} = (i\Omega_{\eta_0} - \Delta)Z + h(r_3)\left(1 + \kappa_2 + Z^2\right) - \sigma^2\left(\frac{1}{2}(1+Z)^3 + \frac{3}{2}(1+Z)\kappa_2 + \kappa_3\right), \quad (32)$$

$$\dot{\kappa}_2 = 2(i\Omega_{\eta_0} - \Delta)\kappa_2 + 4h(r_3)\left(\kappa_3 + Z\kappa_2\right) - \sigma^2\left(\frac{1}{2}(1+Z)^4 + 6(1+Z)^2\kappa_2 + 10(1+Z)\kappa_3 + \frac{9}{2}\kappa_2^2\right). \quad (33)$$

G. Firing rate and the average voltage in the vicinity of the Ott–Antonsen manifold

Montbrió *et al.*[5] reported the firing rate $r(t)$ and $v = \int v_\eta g(\eta)\mathrm{d}\eta$ for arbitrary $w(\phi) = \frac{1}{2\pi}\mathrm{Re}[1 + 2Ze^{-i\phi} + 2\sum_{m=2}^{\infty} z_m e^{-im\phi}]$ [Eq. (B2) in Ref. 5], $r(t) = \pi^{-1}\mathrm{Re}\,W(t)$, and $v(t) = -\mathrm{Im}\,W(t)$,

$$W(t) = 1 - 2Z(t) + 2z_2(t) - 2z_3(t) + \cdots.$$

We calculate z_m (and $Z = z_1$) for the case of enhanced accuracy, where one approximately accounts for κ_3 and decreases inaccuracy to $\mathcal{O}(\sigma^6)$ (recall, generally $\kappa_m \sim \sigma^{2(m-1)}$). With terms up to σ^6, the

circular cumulant-generating function $\Psi(k) = \kappa_1 k + \kappa_2 k^2 + \kappa_3 k^3 + \cdots$, and, as $\Psi(k) = k\partial_k \ln F(k)$, one finds $\ln F = \kappa_1 k + \kappa_2 \frac{k^2}{2} + \kappa_3 \frac{k^3}{3} + \cdots$ and

$$\begin{aligned} F = e^{\ln F} &= e^{\kappa_1 k} e^{\kappa_2 \frac{k^2}{2} + \kappa_3 \frac{k^3}{3} + \cdots} \\ &= e^{\kappa_1 k}\left(1 + \frac{\kappa_2}{2}k^2 + \frac{\kappa_3}{3}k^3 + \frac{\kappa_2^2}{8}k^4 + \mathcal{O}(\kappa_2^3, \kappa_3^2, \kappa_4)\right) \\ &= \sum_{m=0}^{\infty} \kappa_1^m \frac{k^m}{m!}\left(1 + \frac{\kappa_2}{2}k^2 + \frac{\kappa_3}{3}k^3 + \frac{\kappa_2^2}{8}k^4 + \cdots\right). \end{aligned} \tag{34}$$

Since $\sum_{m=0}^{\infty} \kappa_2 \kappa_1^m \frac{k^{m+2}}{m!} = \sum_{m=0}^{\infty} m(m-1)\kappa_2 \kappa_1^{m-2} \frac{k^m}{m!}$, etc., one finds

$$\begin{aligned} z_m &= \kappa_1^m + \frac{m(m-1)}{2}\kappa_2 \kappa_1^{m-2} + \frac{m(m-1)(m-2)}{3}\kappa_3 \kappa_1^{m-3} \\ &\quad + \frac{m(m-1)(m-2)(m-3)}{8}\kappa_2^2 \kappa_1^{m-4} + \cdots \\ &= \left(1 + \frac{\kappa_2}{2}\frac{\mathrm{d}^2}{\mathrm{d}\kappa_1^2} + \frac{\kappa_3}{3}\frac{\mathrm{d}^3}{\mathrm{d}\kappa_1^3} + \frac{\kappa_2^2}{8}\frac{\mathrm{d}^4}{\mathrm{d}\kappa_1^4} + \cdots\right)\kappa_1^m. \end{aligned} \tag{35}$$

Hence,

$$\begin{aligned} W &= 1 - 2Z + 2z_2 - 2z_3 + \cdots \\ &= \left(1 + \frac{\kappa_2}{2}\frac{\mathrm{d}^2}{\mathrm{d}\kappa_1^2} + \frac{\kappa_3}{3}\frac{\mathrm{d}^3}{\mathrm{d}\kappa_1^3} + \frac{\kappa_2^2}{8}\frac{\mathrm{d}^4}{\mathrm{d}\kappa_1^4} + \cdots\right) \\ &\quad \times \left(1 - 2\kappa_1 + 2\kappa_1^2 - 2\kappa_1^3 + \cdots\right) \\ &= \left(1 + \frac{\kappa_2}{2}\frac{\mathrm{d}^2}{\mathrm{d}\kappa_1^2} + \frac{\kappa_3}{3}\frac{\mathrm{d}^3}{\mathrm{d}\kappa_1^3} + \frac{\kappa_2^2}{8}\frac{\mathrm{d}^4}{\mathrm{d}\kappa_1^4} + \cdots\right)\frac{1-\kappa_1}{1+\kappa_1} \\ &= \frac{1-\kappa_1}{1+\kappa_1} + \frac{2\kappa_2}{(1+\kappa_1)^3} - \frac{4\kappa_3}{(1+\kappa_1)^4} + \frac{6\kappa_2^2}{(1+\kappa_1)^5} + \mathcal{O}(\sigma^6). \end{aligned} \tag{36}$$

For the first four orders of expansion,

$$\begin{aligned} W &= W_0 + W_1 + W_2 + W_3 + \mathcal{O}(\sigma^8), \\ W_0 &= \frac{1-\kappa_1}{1+\kappa_1}, \\ W_1 &= \frac{2\kappa_2}{(1+\kappa_1)^3}, \\ W_2 &= \frac{6\kappa_2^2}{(1+\kappa_1)^5} - \frac{4\kappa_3}{(1+\kappa_1)^4}, \\ W_3 &= \frac{30\kappa_2^3}{(1+\kappa_1)^7} - \frac{40\kappa_2\kappa_3}{(1+\kappa_1)^6} + \frac{12\kappa_4}{(1+\kappa_1)^5}. \end{aligned} \tag{37}$$

Specifically, for the Gaussian-friendly closure $\kappa_3 = \frac{3}{2}\frac{\kappa_2^2}{\kappa_1}$,

$$W = \frac{1-\kappa_1}{1+\kappa_1} + \frac{2\kappa_2}{(1+\kappa_1)^3} - \frac{6\kappa_2^2}{\kappa_1(1+\kappa_1)^5} + \mathcal{O}(\sigma^6), \tag{38}$$

which is Eq. (10).

In Fig. 5, one can assess the contribution of different terms W_n into the firing rate for time-independent regimes. As demonstrated previously,[36] the expansion for W should be calculated consistently; for instance, one should not include the κ_2^2-term without the κ_3-term or the κ_2^3-term without the $\kappa_2\kappa_3$- and κ_4-terms, etc. An inconsistent

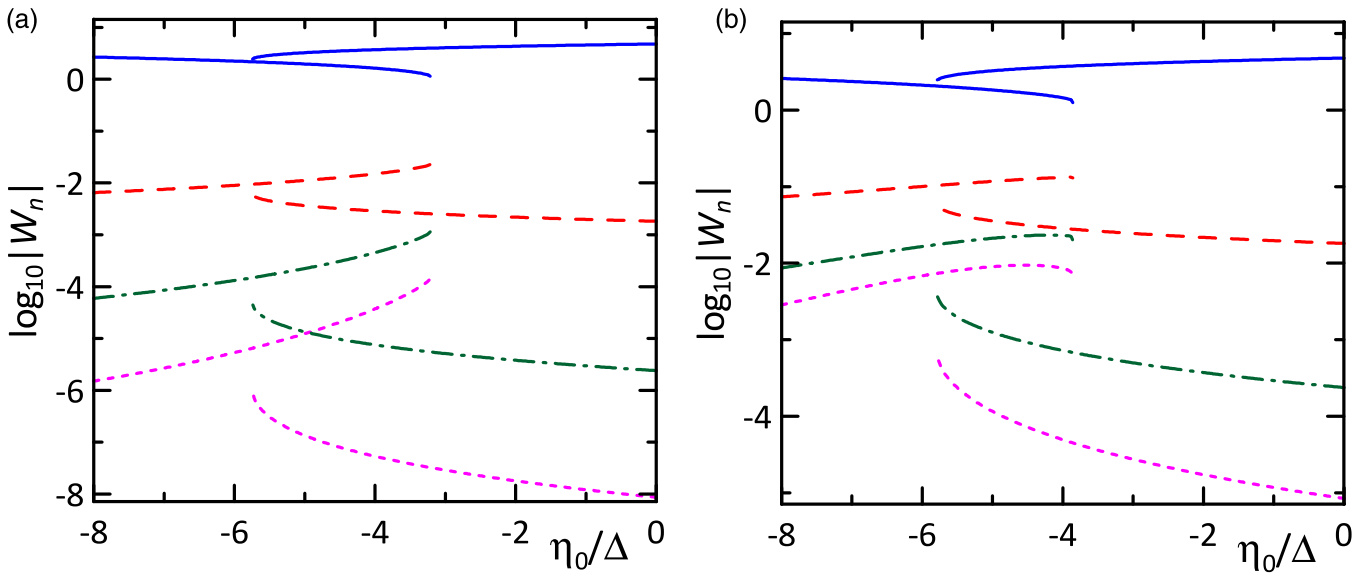

FIG. 5. Cumulant expansion for mean field $W(t)$ (37) for $J/\Delta^{1/2} = 15$, $\sigma^2/\Delta^{3/2} = 0.1$ (a) and 1 (b) for the left and right branches of the "exact" solution. Solid lines: W_0, dashed lines: W_1, dashed–dotted lines: W_2, and dotted lines: W_3.

inclusion of these terms does not enhance the accuracy and, more importantly, leads to the divergence for a long series.

IV. CONCLUSION

For the population of globally coupled quadratic integrate-and-fire neurons (QIFs) subject to noise, we have derived the infinite chain of circular cumulant equations describing the population dynamics beyond the Ott–Antonsen or Montbrió–Pazó–Roxin *Ansätze*. For the series of circular cumulants, we identify the hierarchy of smallness, which allows one to truncate the equation chain. We have presented the results for several two-cumulant model reductions with different closures for higher cumulants κ_3 and κ_4.

We have found that the minimalistic two-cumulant reduction (11) and (12) with firing rate (9) and the enhanced two-cumulant reduction (26) and (27) with (9) yield mostly similar accuracy (Fig. 4). The latter is only slightly more accurate for weak noise and almost by one order of magnitude more accurate for strong noise. However, the behavior for moderate and strong noise can be system-specific, and this result may vary for other networks. The Gaussian closure for κ_3 and κ_4 does not increase accuracy compared to the enhanced two-cumulant reduction. We have also tested the two-cumulant reduction (32) and (33) with quasi-static approximation (30) for κ_3 and firing rate (31). For time-independent states, this reduction works as a three-cumulant model; in Fig. 4, the scaling of its error follows the σ^6-law. The scaling laws of the error for finite-cumulant reductions in Fig. 4 can also be treated as a confirmation of the correctness of the derivations, as the mistakes in coefficients of any terms lower the error order and significantly increase its value.

We have studied the bistability between time-independent regimes with high and low firing rates in a network of coupled sub-threshold QIFs ($\eta_0 < 0$) in the presence of noise. The noise shrinks the bistability domain (Figs. 1 and 2); the main impact is on the low firing rate regime, where noise makes the firing events more frequent and tends to destroy this state.

An important limitation of our accuracy tests is that we considered only heterogeneous populations with a Lorentzian distribution of η. The case of a homogeneous population can be generally featured by a different hierarchy of smallness of κ_m and a different accuracy of the same model reductions. Furthermore, the accuracy for time-dependent regimes[7] can be different as compared to the case of time-independent regimes, although the dynamics of relaxation to the regimes in Fig. 1 were correctly captured by the two-cumulant models.

The approach can be used for a regular derivation of mass models for other networks of QIFs or theta neurons.

ACKNOWLEDGMENTS

The author is thankful to A. Torcini, M. di Volo, L. S. Klimenko, K. Pyragas, and A. Pikovsky for fruitful discussions and comments and acknowledges the financial support from a joint Russian Science Foundation (RSF)–Deutsche Forschungsgemeinschaft (DFG) project (RSF Grant No. 19-42-04120).

DATA AVAILABILITY

The data that support the findings of this study are available within the article.

REFERENCES

[1] T. B. Luke, E. Barreto, and P. So, "Complete classification of the macroscopic behavior of a heterogeneous network of theta neurons," Neural Comput. **25**, 3207 (2013).
[2] C. R. Laing, "Derivation of a neural field model from a network of theta neurons," Phys. Rev. E **90**(1), 010901 (2014).
[3] C. R. Laing, "Exact neural fields incorporating gap junctions," SIAM J. Appl. Dyn. Syst. **14**(4), 1899 (2015).
[4] D. Pazó and E. Montbrió, "Low-dimensional dynamics of populations of pulse-coupled oscillators," Phys. Rev. X **4**, 011009 (2014).
[5] E. Montbrió, D. Pazó, and A. Roxin, "Macroscopic description for networks of spiking neurons," Phys. Rev. X **5**, 021028 (2015).
[6] M. di Volo and A. Torcini, "Transition from asynchronous to oscillatory dynamics in balanced spiking networks with instantaneous synapses," Phys. Rev. Lett. **121**, 128301 (2018).
[7] M. di Volo, M. Segneri, D. S. Goldobin, A. Politi, and A. Torcini, "Emergence of collective oscillations in balanced neural networks due to endogeneous fluctuations " (unpublished) (2021).
[8] I. Ratas and K. Pyragas, "Noise-induced macroscopic oscillations in a network of synaptically coupled quadratic integrate-and-fire neurons," Phys. Rev. E **100**, 052211 (2019).
[9] T. Zheng, K. Kotani, and Y. Jimbo, "Distinct efects of heterogeneity and noise on gamma oscillation in a model of neuronal network with diferent reversal potential," Sci. Rep. **11**, 12960 (2021).
[10] H. Bi, M. Segneri, M. di Volo, and A. Torcini, "Coexistence of fast and slow gamma oscillations in one population of inhibitory spiking neurons," Phys. Rev. Res. **2**, 013042 (2020).
[11] B. Pietras and A. Daffertshofer, "Network dynamics of coupled oscillators and phase reduction techniques," Phys. Rep. **819**, 1 (2019).
[12] V. Klinshov, S. Kirillov, and V. Nekorkin, "Reduction of the collective dynamics of neural populations with realistic forms of heterogeneity," Phys. Rev. E **103**, L040302 (2021).
[13] D. G. Zakharov, M. Krupa, B. S. Gutkin, and A. S. Kuznetsov, "High-frequency forced oscillations in neuronlike elements," Phys. Rev. E **97**, 062211 (2018).
[14] M. Rooy, N. A. Novikov, D. G. Zakharov, and B. S. Gutkin, "Interaction between PFC neural networks ultraslow fluctuations and brain oscillations," Izv. VUZ Appl. Nonlinear Dynam. **28**(1), 90 (2020).
[15] E. Ott and T. M. Antonsen, "Low dimensional behavior of large systems of globally coupled oscillators," Chaos **18**, 037113 (2008).
[16] E. Ott and T. M. Antonsen, "Long time evolution of phase oscillator systems," Chaos **19**, 023117 (2009).
[17] S. Watanabe and S. H. Strogatz, "Constant of motion for superconducting Josephson arrays," Phys. D **74**, 197 (1994).
[18] A. Pikovsky and M. Rosenblum, "Partially integrable dynamics of hierarchical populations of coupled oscillators," Phys. Rev. Lett. **101**, 2264103 (2008).
[19] S. A. Marvel, R. E. Mirollo, and S. H. Strogatz, "Identical phase oscillators with global sinusoidal coupling evolve by Möbius group action," Chaos **19**, 043104 (2009).
[20] C. C. Gong, C. Zheng, R. Toenjes, and A. Pikovsky, "Repulsively coupled Kuramoto–Sakaguchi phase oscillators ensemble subject to common noise," Chaos **29**, 033127 (2019).
[21] E. Rybalova, V. S. Anishchenko, G. I. Strelkova, and A. Zakharova, "Solitary states and solitary state chimera in neural networks," Chaos **29**, 071106 (2019).
[22] E. Rybalova, A. Bukh, G. Strelkova, and V. Anishchenko, "Spiral and target wave chimeras in a 2D lattice of map-based neuron models," Chaos **29**, 101104 (2019).
[23] N. Semenova, A. Zakharova, V. Anishchenko, and E. Schöll, "Coherence–resonance chimeras in a network of excitable elements," Phys. Rev. Lett. **117**, 014102 (2016).
[24] N. Semenova, A. Zakharova, E. Schöll, and V. Anishchenko, "Does hyperbolicity impede emergence of chimera states in networks of nonlocally coupled chaotic oscillators?," Europhys. Lett. **112**, 40002 (2015).
[25] I. A. Shepelev, T. E. Vadivasova, A. V. Bukh, G. I. Strelkova, and V. S. Anishchenko, "New type of chimera structures in a ring of bistable FitzHugh–Nagumo oscillators with nonlocal interaction," Phys. Lett. A **381**, 1398 (2017).

[26]S. A. Bogomolov, A. V. Slepnev, G. I. Strelkova, E. Schöll, and V. S. Anishchenko, "Mechanisms of appearance of amplitude and phase chimera states in ensembles of nonlocally coupled chaotic systems," Commun. Nonlinear Sci. Numer. Simul. **43**, 25 (2017).
[27]Z. P. Kilpatrick and B. Ermentrout, "Sparse gamma rhythms arising through clustering in adapting neuronal networks," PLoS Comput. Biol. **7**(11), e1002281 (2011).
[28]D. Zakharov, M. Krupa, and B. Gutkin, "Modeling dopaminergic modulation of clustered gamma rhythms," Commun. Nonlinear Sci. Numer. Simul. **82**, 105086 (2020).
[29]N. Brunel and V. Hakim, "Fast global oscillations in networks of integrate-and-fire neurons with low firing rates," Neural Comput. **11**, 1621 (1999).
[30]N. Brunel, "Dynamics of sparsely connected networks of excitatory and inhibitory spiking neurons," J. Comput. Neurosci. **8**, 183 (2000).
[31]E. M. Izhikevich, *Dynamical Systems in Neuroscience* (MIT Press, Cambridge, MA, 2007).
[32]G. B. Ermentrout and N. Kopell, "Parabolic bursting in an excitable system coupled with a slow oscillation," SIAM J. Appl. Math. **46**, 233 (1986).
[33]D. S. Goldobin, M. di Volo, and A. Torcini, "A reduction methodology for fluctuation driven population dynamics," Phys. Rev. Lett. **127**, 038301 (2021).
[34]I. V. Tyulkina, D. S. Goldobin, L. S. Klimenko, and A. Pikovsky, "Dynamics of noisy oscillator populations beyond the Ott-Antonsen ansatz," Phys. Rev. Lett. **120**, 264101 (2018).
[35]D. S. Goldobin, I. V. Tyulkina, L. S. Klimenko, and A. Pikovsky, "Collective mode reductions for populations of coupled noisy oscillators," Chaos **28**, 101101 (2018).
[36]D. S. Goldobin and A. V. Dolmatova, "Ott-Antonsen ansatz truncation of a circular cumulant series," Phys. Rev. Res. **1**, 033139 (2019).
[37]I. V. Tyulkina, D. S. Goldobin, L. S. Klimenko, and A. S. Pikovsky, "Two-bunch solutions for the dynamics of Ott-Antonsen phase ensembles," Radiophys. Quantum Electron. **61**(8–9), 640–649 (2019).
[38]D. S. Goldobin, "Relationships between the distribution of Watanabe-Strogatz variables and circular cumulants for ensembles of phase elements," Fluct. Noise Lett. **18**(2), 1940002 (2019).
[39]D. S. Goldobin and A. V. Dolmatova, "Circular cumulant reductions for macroscopic dynamics of Kuramoto ensemble with multiplicative intrinsic noise," J. Phys. A: Math. Theor. **53**, 08LT01 (2020).
[40]V. V. Klinshov, D. A. Zlobin, B. S. Maryshev, and D. S. Goldobin, "Effect of noise on the collective dynamics of a heterogeneous population of active rotators," Chaos **31**, 043101 (2021).
[41]R. Gallego, E. Montbrió, and D. Pazó, "Synchronization scenarios in the Winfree model of coupled oscillators," Phys. Rev. E **96**, 042208 (2017).
[42]J. M. Esnaola-Acebes, A. Roxin, D. Avitabile, and E. Montbrió, "Synchrony-induced modes of oscillation of a neural field model," Phys. Rev. E **96**, 052407 (2017).
[43]C. R. Laing and O. Omel'chenko, "Moving bumps in theta neuron networks," Chaos **30**, 043117 (2020).
[44]C. R. Laing, Ch. Blasche, and Sh. Means, "Dynamics of structured networks of Winfree oscillators," Front. Syst. Neurosci. **15**, 631377 (2021).
[45]C. R. Laing, "The effects of degree distributions in random networks of type-I neurons," Phys. Rev. E **103**, 052305 (2021).
[46]H. Daido, "Onset of cooperative entrainment in limit-cycle oscillators with uniform all-to-all interactions: Bifurcation of the order function," Phys. D **91**, 24 (1996).
[47]E. Lukacs, *Characteristic Functions* (Griffin, London, 1970).
[48]A. N. Malahov, *Cumulant Analysis of Random Non-Gaussian Processes and Their Transformations [in Russian]* (Soviet Radio, Moscow, 1978).
[49]E. I. Yakubovich, "Dynamics of processes in media with inhomogeneous broadening of the line of the working transition," Sov. Phys. JETP **28**(1), 160 (1969).
[50]M. I. Rabinovich and D. I. Trubetskov, *Oscillations and Waves: In Linear and Nonlinear Systems* (Springer Netherlands, 1989).
[51]J. D. Crawford, "Amplitude expansions for instabilities in populations of globally-coupled oscillators," J. Stat. Phys. **74**(5–6), 1047 (1994).